

ChemComm

Chemical Communications

Accepted Manuscript

This article can be cited before page numbers have been issued, to do this please use: P. Wang, X. Jiang and P. Guo, *Chem. Commun.*, 2024, DOI: 10.1039/D4CC03511A.



This is an Accepted Manuscript, which has been through the Royal Society of Chemistry peer review process and has been accepted for publication.

Accepted Manuscripts are published online shortly after acceptance, before technical editing, formatting and proof reading. Using this free service, authors can make their results available to the community, in citable form, before we publish the edited article. We will replace this Accepted Manuscript with the edited and formatted Advance Article as soon as it is available.

You can find more information about Accepted Manuscripts in the [Information for Authors](#).

Please note that technical editing may introduce minor changes to the text and/or graphics, which may alter content. The journal's standard [Terms & Conditions](#) and the [Ethical guidelines](#) still apply. In no event shall the Royal Society of Chemistry be held responsible for any errors or omissions in this Accepted Manuscript or any consequences arising from the use of any information it contains.

COMMUNICATION

Luminescent Macroporous Aerogels of Two-Dimensional Nanocrystals of Metal Halide Perovskites with Adjustable Semiconducting Bandgaps

Penghao Guo,^a Xuelian Jiang^a and Pei-Xi Wang^{*a}Received 00th January 20xx,
Accepted 00th January 20xx

DOI: 10.1039/x0xx00000x

In semiconducting aerogels, exciton-photon interactions occur in porous frameworks with solid-gas interfaces. Herein, by freezing and vacuum freeze-drying of cyclohexane dispersions of platelet-shaped nanocrystals of organic-inorganic metal halide perovskites, aerogels with macro-/meso-porosity, tunable luminescence in the visible light range, and photocurrent responses were fabricated.

As a class of solid materials with high specific surface areas, low bulk densities, and interconnected porosity, aerogels have been used in thermal insulation,¹ acoustic insulation,² batteries,³ catalysis,⁴ and many other fields. The combination of aerogels with luminescence or semiconductivity allows determination of the chemical properties and amounts of guest molecules or ions adsorbed in pores and channels, thus enabling applications in displays,⁵ gas sensors,⁶ pollution monitoring systems,⁷ etc. Non-luminescent aerogels may acquire light-emitting features by incorporating fluorescent dyes,⁸ quantum dots,⁹ rare-earth elements,¹⁰ or semiconducting nanoparticles.¹¹ Aerogels may also be fabricated from intrinsically luminescent microscopic building blocks such as Y₂O₃ nanosheets,¹² chalcogenides,¹³ and CdSe/CdS nanocrystals.¹⁴ To further extend the application range of luminescent aerogels, building blocks with broadly and precisely tunable emission wavelengths, high quantum yields, as well as high color purity would be necessary.

In recent years, layered hybrid organic-inorganic metal halide perovskites (R-NH₃)₂MX₄, a family of solution-processable ionic semiconductors that could be used in optoelectronics and light sources,¹⁵ have attracted much attention due to their structural and compositional diversity.¹⁶ By varying the interlayer organic ammonium cations (R-NH₃⁺) as well as the divalent metal cations (M²⁺ = Pb²⁺, Sn²⁺, Mn²⁺, etc.) and halide anions (X⁻ = Cl⁻,

Br⁻, or I⁻) at the centers and corners of MX₆²⁻ octahedral units, perovskites with different emission wavelengths ranging from near ultraviolet to near infrared may be synthesized.¹⁷ In this research, perovskites were used as construction units of three-dimensional macro- and mesoporous frameworks, where by using cyclohexane (C₆H₁₂) that has a relatively high triple-point temperature of 279.47 K with a vapor pressure of 5.388 kPa,¹⁸ colloidal dispersions of two-dimensional nanocrystals of layered metal halide perovskites were transformed into aerogels after freezing and vacuum freeze-drying. Semiconducting bandgaps of perovskite nanoplatelets were adjusted with the introduction of doping elements, thus enabling the fabrication of aerogels showing photoluminescence with blue, green, and red colors. Photocurrents of the perovskite aerogels were primarily tested under irradiation of ultraviolet and visible light, revealing tunable responsiveness to photons of different frequencies. These results suggest a new approach to aerogels with desired semiconducting bandgaps, and may guide the development of other semiconductive materials with porosity.

In our experiments, a two-dimensional lead(II) halide perovskite of bis(2-phenylethylammonium) tetrabromoplumbate(II) (C₆H₅-CH₂-CH₂-NH₃)₂PbBr₄ was selected as the model material,¹⁹ the crystals of which were synthesized by cooling a hot (373 K) clear aqueous solution containing hydrobromic acid (8.8 mol/L), lead(II) oxide (0.15 mol/L), and 2-phenylethylamine (0.30 mol/L) to 298 K over 2 hours. Colloidal nanoplatelets were prepared by slowly adding an N,N-dimethylformamide solution (0.30 mL) of (C₆H₅-CH₂-CH₂-NH₃)₂PbBr₄ (1.0 mol/L) into a chlorobenzene solution (10.0 mL, anhydrous) of cis-9-octadecenoic acid (0.1% by volume, 3.151 mmol/L) and cis-1-amino-9-octadecene (0.1% by volume, 3.039 mmol/L) at a stirring speed of 2400 revolutions per minute. About 10 minutes later, the reaction mixture was centrifuged at 9000 rpm for 10 minutes in a sealed centrifuge tube. The supernatant fluid was decanted, and the solids were redispersed in a cyclohexane solution (10.0 mL) of cis-9-octadecenoic acid and cis-1-amino-9-octadecene (0.3% by

^a *i*-Lab, Suzhou Institute of Nano-Tech and Nano-Bionics of the Chinese Academy of Sciences, 398 Ruoshui Road, Suzhou, Jiangsu 215123, P. R. China

* Email: pxwang2020@sinano.ac.cn

† Electronic supplementary information (ESI) available: Experimental methods and additional data. See DOI: 10.1039/x0xx00000x



volume each) by sonication, then the dispersion was centrifuged again at 9000 rpm for 30 minutes to collect solids. This washing procedure was repeated two more times, and the solids were finally redispersed in 1.5 mL of the above-described cyclohexane solution to form a concentrated colloidal suspension. Under scanning electron microscopy (SEM) and atomic force microscopy (AFM), the colloids were observed to be rectangular-shaped two-dimensional nanocrystals with lengths of 500-2000 nm and thicknesses of 30-50 nm (Figure 1a,b and Figure S1). The suspension was frozen in a glass vial (with an internal diameter of 16 mm) at about 77 K using liquid nitrogen, and lightweight aerogels were obtained after vacuum freeze-drying at a temperature of 193 K and a pressure of 5 pascals (Figure 2a). In a typical experiment, a cylindrical aerogel of $(\text{C}_6\text{H}_5\text{-CH}_2\text{-CH}_2\text{-NH}_3)_2\text{PbBr}_4$ showed a diameter of 15.9 mm, a height of 6.8 mm, and a mass of 78.9 mg, corresponding to a macroscopic mass density of about 58.4 milligrams per square centimeter. Under ultraviolet light (wavelength of 365 nm), the aerogels exhibited blue-colored fluorescence (Figure 2b), and photoluminescence spectroscopy (excitation wavelength at 365 nm) revealed a single emission peak at 413 nm (Figure 3a).

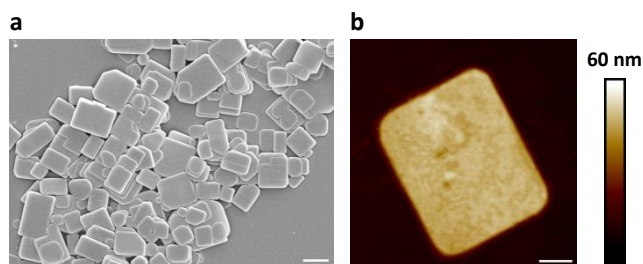


Fig. 1. SEM (a) and AFM (b) images of $(\text{C}_6\text{H}_5\text{-CH}_2\text{-CH}_2\text{-NH}_3)_2\text{PbBr}_4$ nanoplatelets. Scale bars: (a) 1 μm , (b) 200 nm.

By using an *N,N*-dimethylformamide solution (0.30 mL) of $(\text{C}_6\text{H}_5\text{-CH}_2\text{-CH}_2\text{-NH}_3)_2\text{PbBr}_4$ (1.0 mol/L) and manganese(II) bromide (0.2 mol/L) during the antisolvent-induced micro-precipitation process, colloidal nanoplatelets of manganese(II)-doped $(\text{C}_6\text{H}_5\text{-CH}_2\text{-CH}_2\text{-NH}_3)_2\text{PbBr}_4$ perovskites were synthesized (Figure S2). After liquid-nitrogen freezing at 77 K and vacuum freeze-drying, aerogels were fabricated (Figure 2c), showing an actual doping concentration of 2.3 mol% manganese(II) as analyzed by inductively coupled plasma-optical emission spectroscopy (ICP-OES), a bulk mass density of about 113.3 mg/cm^3 , red-colored fluorescence under 365-nm ultraviolet light (Figure 2d), dual-band emission with two peaks at wavelengths of 412 nm and 598 nm (Figure 3a), and a photoluminescence quantum yield of 2.6%, which was slightly higher than the 1.1% PLQY of aerogels formed by undoped $(\text{C}_6\text{H}_5\text{-CH}_2\text{-CH}_2\text{-NH}_3)_2\text{PbBr}_4$ nanoplatelets. By mixing $(\text{C}_6\text{H}_5\text{-CH}_2\text{-CH}_2\text{-NH}_3)_2\text{PbBr}_4$ (1.00 mol/L) and $(\text{C}_6\text{H}_5\text{-CH}_2\text{-CH}_2\text{-NH}_3)_2\text{PbI}_4$ (0.33 mol/L) in the DMF precursor solution (0.30 mL), $(\text{C}_6\text{H}_5\text{-CH}_2\text{-CH}_2\text{-NH}_3)_2\text{PbBr}_3\text{I}$ nanoplatelets (Figure S3) and aerogels were prepared (Figure 2e), where the aerogels exhibited a macroscopic mass density of 66.7 mg/cm^3 , green fluorescence under 365-nm light (Figure 2f), a single emission peak at 496 nm (Figure 3a), and a quantum yield of 10.5%. Powder X-ray diffraction patterns of fine powders of the above

three perovskite aerogels revealed periodically spaced peaks matching those in simulated diffraction patterns calculated from the single-crystal X-ray crystallography data of $(\text{C}_6\text{H}_5\text{-CH}_2\text{-CH}_2\text{-NH}_3)_2\text{PbBr}_4$ (Figure 3b).²⁰ In doped aerogels, Mn^{2+} and I^- were detected by X-ray photoelectron spectroscopy (Figure S4).

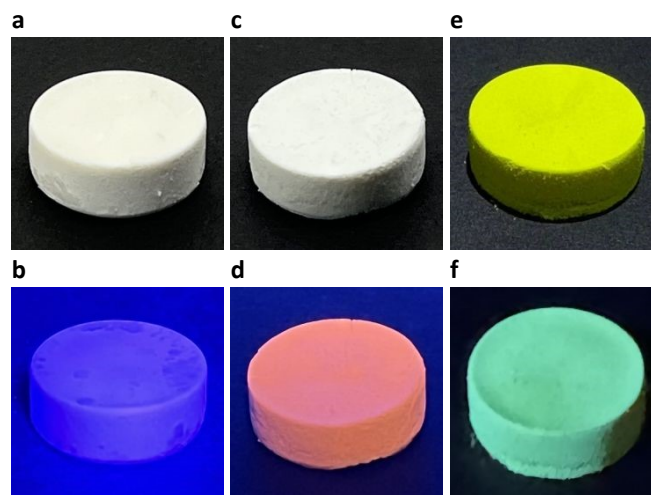


Fig. 2. Photographs of $(\text{C}_6\text{H}_5\text{-CH}_2\text{-CH}_2\text{-NH}_3)_2\text{PbBr}_4$ (a,b), $(\text{C}_6\text{H}_5\text{-CH}_2\text{-CH}_2\text{-NH}_3)_2\text{Pb}_{0.977}\text{Mn}_{0.023}\text{Br}_4$ (c,d), and $(\text{C}_6\text{H}_5\text{-CH}_2\text{-CH}_2\text{-NH}_3)_2\text{PbBr}_3\text{I}$ (e,f) aerogels under white (a,c,e) and 365-nm ultraviolet light (b,d,f). Diameters of the aerogels were 16 mm.

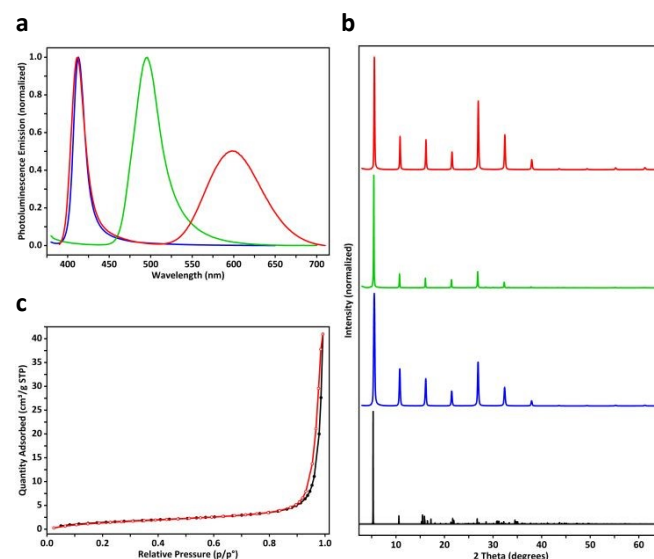


Fig. 3. (a,b) Emission spectra (a) and PXR patterns (b) of $(\text{C}_6\text{H}_5\text{-CH}_2\text{-CH}_2\text{-NH}_3)_2\text{PbBr}_4$ (blue; simulated PXR profile depicted in black), $(\text{C}_6\text{H}_5\text{-CH}_2\text{-CH}_2\text{-NH}_3)_2\text{PbBr}_3\text{I}$ (green), and $(\text{C}_6\text{H}_5\text{-CH}_2\text{-CH}_2\text{-NH}_3)_2\text{Pb}_{0.977}\text{Mn}_{0.023}\text{Br}_4$ (red) aerogels. (c) Nitrogen adsorption-desorption isotherms of $(\text{C}_6\text{H}_5\text{-CH}_2\text{-CH}_2\text{-NH}_3)_2\text{PbBr}_4$ aerogels.

Nitrogen adsorption-desorption isotherms of a $(\text{C}_6\text{H}_5\text{-CH}_2\text{-CH}_2\text{-NH}_3)_2\text{PbBr}_4$ aerogel revealed a BET specific surface area of 5.83 m^2/g and a BJH adsorption average pore width (4V/A) of 42.5 nm (Figure 3c), while BET specific surface areas of iodine- and manganese-doped perovskite aerogels were measured to be



1.87 and 4.46 m²/g (Figure S5), respectively. The relatively low surface areas may be caused by the large sizes of cyclohexane microcrystals.²¹ Cross-sectional SEM images of (C₆H₅-CH₂-CH₂-NH₃)₂PbBr₄ aerogels showed hierarchical structures created by frozen and then sublimed cyclohexane microcrystals. At low magnifications, parallel porous channels with millimeter-scale directional orderliness were observed (Figure 4a), indicating local propagation directions of solidified cyclohexane during freezing. Frameworks of the aerogels were composed mainly of chamber-like macropores with diameters of 30-50 microns (Figure 4b), and these chambers were further interconnected by micro-holes with widths of 5-20 μm (Figure 4c,d). At higher magnifications, walls of the macropores were found to consist of aggregated perovskite nanoplatelets with rectangular geometry (Figure 4e,f and Figure S6). Under SEM, aerogels of doped perovskites (C₆H₅-CH₂-CH₂-NH₃)₂Pb_{0.977}Mn_{0.023}Br₄ and (C₆H₅-CH₂-CH₂-NH₃)₂PbBr₃I₁ exhibited similar structures of unidirectionally ordered micro-channels and three-dimensional porous frameworks (Figure S7,S8), suggesting that freezing and vacuum freeze-drying of colloidal cyclohexane dispersions of perovskites could efficiently transform them into aerogels.

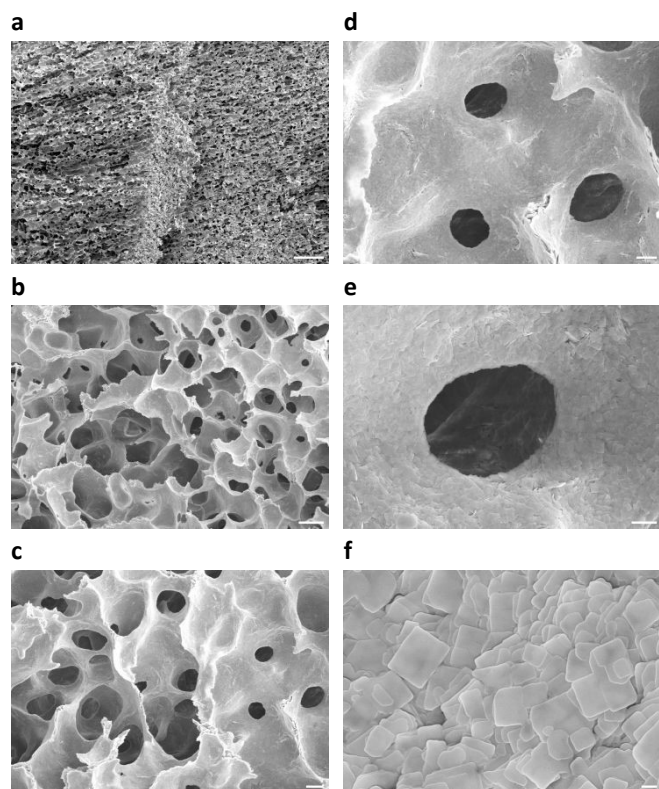


Fig. 4. Cross-sectional SEM images of a (C₆H₅-CH₂-CH₂-NH₃)₂PbBr₄ aerogel. Scale bars: (a) 200 μm, (b) 50 μm, (c) 20 μm, (d) 10 μm, (e) 4 μm, (f) 500 nm.

Electrical and photoelectric properties of the aerogels were evaluated by using transparent interdigitated electrodes made of indium tin oxide on glass, each of which had a digit length of 13 mm, a digit width of 0.2 mm, an inter-digit spacing distance of 0.2 mm, and 16 pairs of digits. Measurements of current-

voltage characteristics were conducted in the dark and under illumination (0.18 mW/mm²), where photocurrents of perovskite aerogels were approximately 1000 times higher than the corresponding dark currents (Figure 5a and Figure S9). Time-resolved photocurrent responses of perovskite aerogels were examined under pulsed laser irradiation with different powers (Figure 5b), revealing reproducible and abrupt on-off switching behaviors. During a typical on-off switch cycle, a (C₆H₅-CH₂-CH₂-NH₃)₂PbBr₄ aerogel showed rise and decay times (10% - 90%) less than 40 milliseconds (Figure 5c). Responsivity of perovskite aerogels to photons of different wavelengths was dependent on their compositions. (C₆H₅-CH₂-CH₂-NH₃)₂PbBr₃I₁ aerogels with green emission and narrower energy bandgaps exhibited greater sensitivity to 500-nm light, and produced relatively higher photocurrents than those detected in undoped blue-emitting (C₆H₅-CH₂-CH₂-NH₃)₂PbBr₄ aerogels; while Mn²⁺ dopants may increase the density of charge carriers under 365-nm illumination (Figure 5d-f).

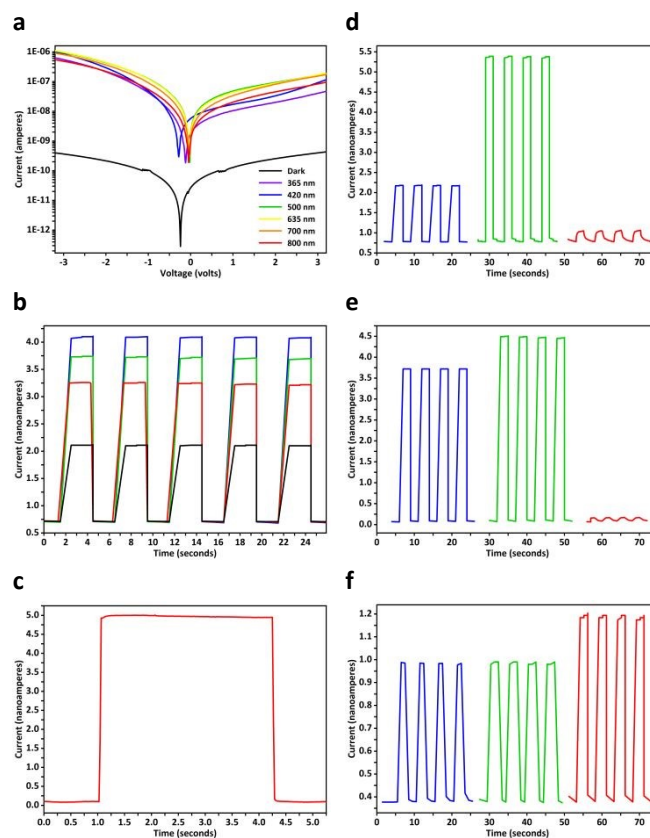


Fig. 5. (a) Current-voltage characteristics of a (C₆H₅-CH₂-CH₂-NH₃)₂PbBr₄ aerogel under 0.18 mW/mm² illumination. (b) Time-resolved photocurrents of a (C₆H₅-CH₂-CH₂-NH₃)₂PbBr₄ aerogel under 365-nm irradiation with power densities of 0.18 (black), 0.35 (red), 0.50 (green), and 0.68 mW/mm² (blue). (c) The rise and decay of the photocurrent in a (C₆H₅-CH₂-CH₂-NH₃)₂PbBr₄ aerogel during an on-off cycle of light (365-nm, 0.68 mW/mm²). (d-f) Time-resolved photocurrents of (C₆H₅-CH₂-CH₂-NH₃)₂PbBr₄ (d), (C₆H₅-CH₂-CH₂-NH₃)₂Pb_{0.977}Mn_{0.023}Br₄ (e), and (C₆H₅-CH₂-CH₂-NH₃)₂PbBr₃I₁ (f) aerogels under 365-nm (blue), 420-nm (green), and 800-nm (red) illumination.



(green), and 500-nm (red) lasers (0.18 mW/mm²). From (b) to (f), a bias voltage of 1 volt was applied to the aerogels.

In summary, semiconducting aerogels with macro-/mesoporosity and tunable luminescence were prepared by freezing and vacuum freeze-drying of nonpolar cyclohexane dispersions of colloidal two-dimensional nanoplatelets of layered organic-inorganic metal halide perovskites. Emission wavelengths of the aerogels were widely regulated by doping elements to achieve fluorescence with blue, green, and red colors. Photoelectronic analysis of perovskite aerogels under visible and ultraviolet light revealed transient photocurrent responses and reproducible on-off switching behaviors. With porous spatial frameworks, high specific surface areas, and adjustable energy bandgaps, these hierarchically structured semiconductors may be used for gas sensing, catalysis, or long-distance diffuse illumination.

This research was supported by the National Natural Science Foundation of China (Young Scientists Fund 22205255), Natural Science Foundation of Jiangsu Province (Young Scientists Fund BK20220297), the Youth Innovation Promotion Association of the Chinese Academy of Sciences (2023336), the Jiangsu Provincial Innovation and Entrepreneurship Talents Program (JSSCRC2022463; JSSCBS20211429), and the Gusu Innovation and Entrepreneurship Leading Talents Program (ZXL2022467).

Conflicts of interest

There are no conflicts to declare.

Data availability

The data supporting this article have been included as part of the Supplementary Information.

Notes and references

¹ S. S. Kistler and A. G. Caldwell, *Ind. Eng. Chem.*, 1934, **26**, 658–662.

² P. P. Narang, *Appl. Acoust.*, 1991, **34**, 249–259.

³ D. B. Le, S. Passerini, A. L. Tipton, B. B. Owens and W. H. Smyrl, *J. Electrochem. Soc.*, 1995, **142**, L102–L103.

⁴ J. B. Miller, S. E. Rankin and E. I. Ko, *J. Catal.*, 1994, **148**, 673–682.

⁵ Z. He, X. Liang and W. Xiang, *Chem. Eng. J.*, 2022, **427**, 130964.

⁶ X. You, J. Wu and Y. Chi, *Anal. Chem.*, 2019, **91**, 5058–5066.

⁷ I. R. Pala and S. L. Brock, *ACS Appl. Mater. Interfaces*, 2012, **4**, 2160–2167.

⁸ N. Leventis, I. A. Elder, D. R. Rolison, M. L. Anderson and C. I.

View Article Online

DOI: 10.1039/D4CC03511A

Merzbacher, *Chem. Mater.*, 1999, **11**, 2837–2845.

⁹ M. Zhang, J. Xue, Y. Zhu, C. Yao and D. Yang, *ACS Appl. Mater. Interfaces*, 2020, **12**, 22191–22199.

¹⁰ F. Liu, L. D. Carlos, R. A. S. Ferreira, J. Rocha, M. C. Gaudino, M. Robitzer and F. Quignard, *Biomacromolecules*, 2008, **9**, 1945–1950.

¹¹ L. Sorensen, G. F. Strouse and A. E. Stiegman, *Adv. Mater.*, 2006, **18**, 1965–1967.

¹² W. Cheng, F. Rechberger and M. Niederberger, *ACS Nano*, 2016, **10**, 2467–2475.

¹³ S. Bag, P. N. Trikalitis, P. J. Chupas, G. S. Armatas and M. G. Kanatzidis, *Science*, 2007, **317**, 490–493.

¹⁴ J. L. Mohanan and S. L. Brock, *J. Non. Cryst. Solids*, 2004, **350**, 1–8.

¹⁵ Y. Chen, Y. Sun, J. Peng, J. Tang, K. Zheng and Z. Liang, *Adv. Mater.*, 2018, **30**, 1703487.

¹⁶ L. Mao, C. C. Stoumpos and M. G. Kanatzidis, *J. Am. Chem. Soc.*, 2019, **141**, 1171–1190.

¹⁷ M. D. Smith, B. A. Connor and H. I. Karunadasa, *Chem. Rev.*, 2019, **119**, 3104–3139.

¹⁸ J. G. Aston, G. J. Szasz and H. L. Fink, *J. Am. Chem. Soc.*, 1943, **65**, 1135–1139.

¹⁹ D. Liang, Y. Peng, Y. Fu, M. J. Shearer, J. Zhang, J. Zhai, Y. Zhang, R. J. Hamers, T. L. Andrew and S. Jin, *ACS Nano*, 2016, **10**, 6897–6904.

²⁰ K. Shibuya, M. Koshimizu, F. Nishikido, H. Saito and S. Kishimoto, *Acta Crystallogr. Sect. E Struct. Reports Online*, 2009, **65**, m1323–m1324.

²¹ D. C. Steytler, B. H. Robinson, J. Eastoe, K. Ibel, J. C. Dore and I. MacDonald, *Langmuir*, 1993, **9**, 903–911.



Data Availability Statements

View Article Online
DOI: 10.1039/D4CC03511A

The data supporting this article have been included as part of the Supplementary Information.

Date: 2024 July 14

Corresponding author: Pei-Xi Wang

